

Article

A Label-Free Impedimetric Genosensor for the Nucleic Acid Amplification-Free Detection of Extracted RNA of Dengue Virus

Ching-Chou Wu ^{1,2,*} , Hao-Yu Yen ¹, Lu-Ting Lai ¹, Guey-Chuen Perng ³, Cheng-Rei Lee ⁴ and Shuenn-Jue Wu ⁴

¹ Department of Bio-industrial Mechatronics Engineering, National Chung Hsing University, No. 145, Xingda Rd., South Dist., Taichung City 402, Taiwan; hugo19810607@hotmail.com (H.-Y.Y.); luting822000@yahoo.com.tw (L.-T.L.)

² Innovation and Development Center of Sustainable Agriculture, National Chung Hsing University, No. 145, Xingda Rd., South Dist., Taichung City 402, Taiwan

³ Department of Microbiology and Immunology, College of Medicine, National Cheng Kung University, No.1, University Rd., Tainan City 701, Taiwan; gperng@mail.ncku.edu.tw

⁴ Viral & Rickettsial Diseases Department, Naval Medical Research Center, Silver Spring, MD 20910, USA; cheng-rei.r.lee.ctr@mail.mil (C.-R.L.); shuenn-jue.l.wu.civ@mail.mil (S.-J.W.)

* Correspondence: ccwu@dragon.nchu.edu.tw; Tel.: +886-4-2285-1268

Received: 26 May 2020; Accepted: 1 July 2020; Published: 3 July 2020



Abstract: Developing rapid and sensitive diagnostic methods for dengue virus (DENV) infection is of prime priority because DENV infection is the most prevalent mosquito-borne viral disease. This work proposes an electrochemical impedance spectroscopy (EIS)-based genosensor for the label-free and nucleic acid amplification-free detection of extracted DENV RNA intended for a sensitive diagnosis of DENV infection. A concentration ratio of 0.04 mM 6-mercaptopentanoic acid (MHA) to 1 mM 6-mercapto-1-hexanol (MCH) was selected to modify thin-film gold electrodes as a link to control the coverage of self-designed probe DNA (pDNA) at a density of $4.5 \pm 0.4 \times 10^{11}$ pDNA/cm². The pDNA/MHA/MCH-modified genosensors are proven to improve the hybridization efficiency of a synthetic 160-mer target DNA (160mtDNA) with a 140-mer electrode side overhang as compared to other MHA/MCH ratio-modified genosensors. The MHA(0.04 mM)/MCH(1 mM)-modified genosensors also present good hybridization efficiency with the extracted DENV serotype 1 (DENV1) RNA samples, having the same electrode side overhangs with the 160mtDNA, showing a low detection limit of 20 plaque forming units (PFU)/mL, a linear range of 10²–10⁵ PFU/mL and good selectivity for DENV1. The pDNA density-controlled method has great promise to construct sensitive genosensors based on the hybridization of extracted DENV nucleic acids.

Keywords: impedimetric genosensor; label-free; probe DNA density; dengue RNA; overhang; nucleic acid amplification-free

1. Introduction

The epidemic of dengue, malaria, chikungunya, yellow fever, West Nile virus and Japanese encephalitis, notorious diseases transmitted by mosquitoes [1], have been propelled by climate warming, globalization and increasing international activity [2–4]. In particular, dengue virus (DENV) infection is the most prevalent mosquito-borne viral disease in tropical and sub-tropical regions covering 40% of the population of the world in 112 countries [1,5]. Infected patients may exhibit asymptomatic, dengue fever [6,7] or severe dengue, such as dengue hemorrhagic fever and dengue shock syndrome [8]. The clinical presentation of dengue fever is similar to many other common febrile diseases making

the correct diagnosis of DENV difficult for attending physicians. Therefore, developing rapid and sensitive diagnostic methods for DENV infection from the onset of febrile symptoms is very important in dengue fever prevention and treatment.

Presently, many strategies have been developed to detect DENV based on the measurement of specific biomarkers of DENV infection, such as soluble non-structural protein 1 (NS1) [9–11], DENV envelope protein [12,13], anti-DENV IgM or IgG antibodies [14] and DENV nucleic acid fragments [15–21] in patient sera. However, the immunoreactive kits cannot differentiate the serotypes of DENV. Primary infection of patients can be caused by any one of the four serotypes of DENV (DENV1, 2, 3, and 4) and secondary infection of these patients with a heterologous serotype increases the risk of progressing into severe dengue due to antibody-dependent enhancement [22,23]. Furthermore, compared with NS1 or anti-DENV IgM, DENV particles are the first to be detected in dengue patient serum post symptom onset [21]. The serotype-specific detection of DENV will be more time-effective for DENV diagnosis and more meaningful for clinical treatments.

Reverse transcription polymerase chain reaction (RT-PCR) and RT loop-mediated isothermal amplification have been widely used for nucleic acid amplification and the diagnosis of the DENV serotypes by using specific primers [24]. However, RT-PCR performance depends on highly trained personnel, well-controlled temperature, expensive instruments and fluorescence-labeled reagents. In contrast, electrochemical DNA genosensors have attracted wide attention for the detection of nucleic acid hybridization in an easy, rapid and inexpensive way. Anusha et al. reviewed the progress of electrochemical genosensors of dengue, classified in amperometry, voltammetry and impedimetry [25]. Experimentally, specific sequences used as probe DNA (pDNA) are immobilized on the surface of various electrodes, and then the electrochemical signal, after hybridization, is directly quantified by electrocatalytic electrodes, such as $\text{Cu}_2\text{CdSnS}_4/\text{O}_2/\text{Si}$ [17], graphite electrode [18] and indium tin oxide (ITO) [26], and evaluated by using electroactive intercalator, such as methylene blue [19,27], and mediators, such as ferrocyanide/ferricyanide [15,16,20,28]. While most publications on electrochemical DNA genosensors used synthetic DNA (≤ 200 -mer) or nucleic acid amplification RNA fragments (< 150 -mer) as the target analytes to elucidate the sensing performance of genosensors [15,17–20,27,28], only one study detected the extracted RNA fragments of DENV [16]. Mills et al. [27] and Lynch III et al. [28] developed four-way junction-based genosensors to solve the influence of overhangs on the detection of synthetic DNA (200-mer) and Zika RNA amplicon (147-mer), respectively. Presently, there is little research exploring the nucleic acid amplification-free detection by a genosensor, because it is difficult to control the total length of directly extracted targets with length-varied overhangs, which may hinder the hybridization efficiency. Jin et al. used the $\text{SiO}_2@3$ -aminopropyltriethoxysilane- functionalized graphene oxide (APTES-GO) modified Pt electrode for pDNA immobilization and measured the increment of interfacial electron transfer resistance (R_{et}) by using electrochemical impedance spectroscopy (EIS) after hybridizing synthetic target DNA (tDNA) or extracted DENV2 RNA at 60 °C for 5 h [16]. Although the label-free EIS-based genosensor had an ultrasensitive detection limit (1 fM) of RNA, the R_{et} signal obtained from the hybridization of 1 fM and 10 pM RNA samples had no significant difference. Moreover, the genosensor did not demonstrate selectivity to different serotypes of DENV. These results show that it is worth the efforts to improve the sensing properties of genosensors for the detection of extracted viral nucleic acids. One of the problems for the genosensors to directly detect the extracted nucleic acids is the difficulty in hybridization of extracted DENV RNA (about 11,000 nucleotides) to the pDNA on a densely pDNA-immobilized genosensor. The excessively long overhangs create the steric and repulsive hindrance on the immobilized pDNA making them inaccessible. Corrigan et al. explored the effect of length-varied solution side overhangs on the hybridization efficiency for the 1.5 μM pDNA(15-mer)-modified genosensors [29]. The EIS signal ratio of hybridizing 30-mer tDNA was larger than that of hybridizing 15, 60 and 100-mer tDNA. Riedel et al. also found that the longer solution side overhangs (10–55-mer) decreased the hybridization efficiency, and the electrode side overhangs (10-mer) also decreased the hybridization [30]. Therefore, developing a genosensor capable

of overcoming the steric hindrance of the overhangs in order to detect the extracted DENV RNA is an important challenge for the development of PCR-free dengue diagnostics. In particular, there are only a few studies to explore the effect of pDNA density on the hybridization efficiency of extracted nucleic acids.

This work proposes a surface-modifying method to adjust the coverage of immobilized pDNA. A binary self-assembled monolayer (SAM) with different ratio of 6-mercaptopentanoic acid (MPA) and 6-mercaptopentanol (MPH) was used as a link for the covalent immobilization of NH₂-terminated pDNA via the activated COOH group of SAM. The relationship between the length of electrode side overhangs and the coverage of pDNA was explored by EIS, and the hybridization efficiency of pDNA coverage-varied genosensors was also discussed. Moreover, the selectivity of genosensors immobilized by DENV1-specific pDNA to different serotypes of DENV was compared.

2. Materials and Methods

2.1. Reagents and Chemicals

Sodium phosphate dibasic, sodium phosphate monobasic dihydrate, tris(hydroxymethyl)aminomethane (Tris), N-[Tris(hydroxymethyl)methyl]-2-aminoethanesulfonic acid (TES), MPA, MPH, N-(3-dimethylaminopropyl)-N'-ethylcarbodiimide hydrochloride (EDC), N-hydroxysuccinimide (NHS), 2-(N-morpholino) ethanesulfonic acid (MES), potassium chloride (KCl), hexammineruthenium(III) chloride and bovine serum albumin (BSA) were purchased from Sigma-Aldrich (St. Louis, MO, USA). Potassium hexacyanoferrate(III) (K₃[Fe(CN)₆]) and potassium hexacyanoferrate(II) trihydrate (K₄[Fe(CN)₆]) 3H₂O were purchased from Showa Chemical (Tokyo, Japan). All chemicals were of reagent grade and were used without further purification. All solutions were prepared with water purified through a Milli-Q system.

2.2. Design and Production of DNA Samples

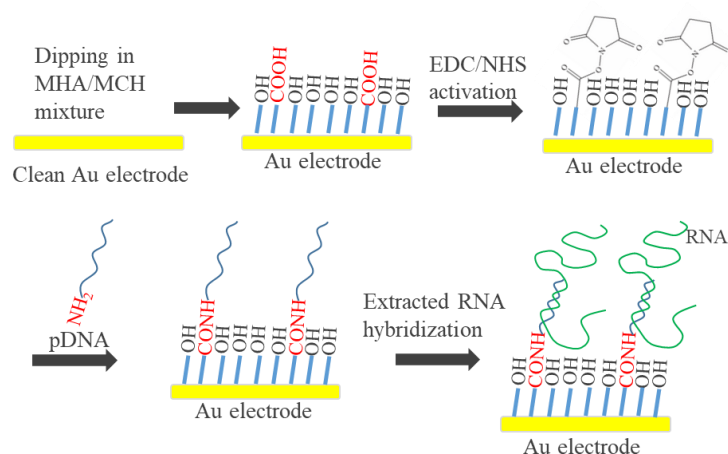
A full-length sequence of DENV1 (Hawaii, KM204119) was obtained from GenBank of National Center for Biotechnology Information (NCBI). Compared with DENV2 (16681, KU725663), DENV3 (H87, M93130) and DENV4 (H241, AY947539), a 20-mer specific sequence, found in DENV1 RNA by a CLC Sequence Viewer (Qiagen Bioinformatics (Redwood, CA)), was identified as target DNA (designated as 20mtDNA) with the sequences of 5'-GTACCCTGGTGGTAAGGACT-3'. The 3' terminus of the 20mtDNA has a 140-mer distance away from the 3' terminus of full-length DENV1 RNA. The corresponding pDNA is completely complementary to the 20mtDNA with the sequences of 5'-AGTCCTTACCACCAGGGTAC-3' and is modified with the NH₂-(CH₂)₆ group at the 5' terminus. In order to realize the effect of electrode side overhang on the hybridization efficiency, a 160-mer target DNA, designated as 160mtDNA, was synthesized according to the last 160-mer sequence from 3' terminus of DENV1 RNA. The sequence of all tDNA and pDNA is shown in Table 1. All DNA strands were synthesized by Genomics (Taiwan) and purified by high performance liquid chromatography.

Table 1. Sequences of pDNA, 20mtDNA and 160mtDNA.

Name	Sequence from 5' to 3' Terminal
pDNA	NH ₂ -(CH ₂) ₆ -AGT CCT TAC CAC CAG GGT AC
Complementary 20mtDNA	GTA CCC TGG TGG TAA GGA CT
160mtDNA	GTA CCC TGG TGG TAA GGA CTA GAG GTT AGA GGA GAC CCC CCG CAC AAC AAT AAA CAG CAT ATT GAC GCT GGG AGA GAC CAG AGA TCC TGC TGT CTC TAC AGC ATC ATT CCA GGC ACA GAA CGC CAG AAA ATG GAA TGG TGC TGT TGA ATC AAC AGG TTC T

2.3. Preparation of Genosensor

30-nm Ti and 200-nm Au thin films were patterned as a rectangular electrode on a cleaned glass substrate by lift-off microfabrication techniques. The working area of electrodes was defined as a disk shape with 1.6 mm in diameter by a 7 μm -thick negative photoresist, SU8-3010 (MicroChem Laboratory, Newton, MA, USA). After cleaning the surface of the Au electrodes, the electrodes were dipped in the mixture of MHA and MCH with concentration-varied ratio for 4 h to form a binary SAM. The preparation of genosensor is shown in Scheme 1. The COOH group of MHA was activated by the mixture of 30 mM EDC and 30 mM NHS prepared in 20 mM MES (pH 4.6) for 1 h. Afterwards, a 10 μL aliquot of 4 μM pDNA and 150 mM NaCl-containing 10 mM phosphate buffer (pH 7.0) was dripped on the activated SAM and incubated at 40 $^{\circ}\text{C}$ for 1 h for covalent immobilization. After rinsing with pure water, the pDNA/MHA/MCH/Au electrodes were used as genosensors. Experimentally, 10 μL aliquot of the concentration-varied 20mtDNA or 160mtDNA was dropped on the genosensors for 60 min at room temperature for hybridization.



Scheme 1. 6-Mercaptohexanoic acid/6-mercapto-1-hexanol (MHA/MCH) modification of the Au electrode followed by N-(3-dimethylaminopropyl)-N'-ethylcarbodiimide hydrochloride/N-hydroxysuccinimide (EDC/NHS) activation, pDNA immobilization and extracted RNA hybridization.

2.4. Measurement of Self-Assembled Monolayer (SAM) Coverage and pDNA Density

The surface coverage of MHA/MCH binary SAM can be quantified via a one-electron reductive path in an alkaline solution (pH ≥ 11) [31]. The reductive equation is represented as follows:



Hence, the amount of reductive charge arising from Au-S desorption can be counted by integrating the reduction current against time ($Q = \int idt$) for the determination of the coverage per cm^2 . The pDNA coverage immobilized at the MHA/MCH-modified electrodes can be calculated by the amount of positively electroactive molecules adsorbed with the negatively charged phosphate group of DNA backbone [32]. In Steel's study the trivalent cation, ruthenium(III) hexaammine (RuHex), had been proved to quantify pDNA density due to the strong electrostatic association between RuHex cation and DNA phosphate in a low ionic strength (IS) electrolyte. The amount of adsorbed RuHex can be measured using chronocoulometry by integrating the reductive current of RuHex. The obtained current is attributed to the diffusion-controlled current, the charging current of the double layer, and the reductive current of adsorbed RuHex. The corresponding charge, Q , is presented in Equation (1).

$$Q = 2nFAD^{1/2}C^*t^{1/2}/\pi^{1/2} + Q_{dl} + nFA\Gamma_0 \quad (1)$$

The first term on the right-hand side is obtained from the integrated Cottrell equation with a linear relation with the square root of time ($t^{1/2}$). Where n ($= 1$) is the electron-transfer number per RuHex for reduction, F is Faraday constant (96485 C/mol), A ($= 0.02 \text{ cm}^2$) is the electrode area, D is the diffusion coefficient of RuHex, C^* is the bulk concentration of RuHex, Q_{dl} is the capacitive charge (C), and Γ_0 is the surface density (mol/cm^2) of adsorbed RuHex. The chronocoulometric intercept at $t = 0$ is the sum of Q_{dl} and $nFA\Gamma_0$. Therefore, the Γ_0 is determined from the difference in chronocoulometric intercepts at $t = 0$ in the presence and absence of RuHex molecules. The pDNA/MHA/MCH/Au genosensors were respectively immersed in 10 mM Tris buffer (pH 7.4) and 50 μM RuHex-containing 10 mM Tris buffer (pH 7.4) to perform a step potential from 0.1 V to -0.4 V for the calculation of Γ_0 . Afterwards, the pDNA surface density can be calculated according to Equation (2).

$$\Gamma_{\text{DNA}} = \Gamma_0(z/m)(N_A) \quad (2)$$

where Γ_{DNA} is the pDNA density ($\text{molecules}/\text{cm}^2$), m ($=20$) is the number of bases in the pDNA, z ($=3$) is the charge of the RuHex molecule, and N_A is Avogadro's number.

2.5. Electrochemical Measurements

Cyclic voltammetry (CV), chronocoulometry and EIS were performed with an IM-6 impedance analyzer (Zahner Elektrik GmbH, Germany) in a three-electrode system. Pt wire and Ag/AgCl electrode were used as the counter electrode and the reference electrode, respectively. The 1 mM equimolar $\text{Fe}(\text{CN})_6^{3-/4-}$ -containing 26 mM TES buffer (pH 7.0) was used to probe the electrochemical properties of the electrode/electrolyte interface. Impedimetric measurement was carried out in the frequency range of 1 Hz to 10 kHz at +0.2 V potential added with a 5 mV amplitude sine wave versus the Ag/AgCl electrode. The IM-6/THALES software package was used for the acquisition of impedance spectra, and the simulation of equivalent circuits.

2.6. Extracted RNA Test

The commercial E.Z.N.A.[®] Viral RNA Kit (Omega Bio-tek (Norcross, GA) was used to extract RNA fragments from DENV1 suspension samples ranged from 10^4 to 10^6 plaque forming units (PFU)/mL, supplied by the laboratory of the co-author, Dr. Perng. A 150 μL aliquot of the DENV sample was first mixed in 500 μL QVL Lysis Buffer for 7 min, and then slightly centrifugalized. 350 μL aliquot of pure ethanol (99.9%) was added in the mixture, vortexed for 30 s, and then slightly centrifuged. The mixture was transferred to HiBind[®] RNA Mini Column and centrifuged at 13,000 g for 15 s. This step was repeated until the residual RNA sample was fully transferred to the column. Subsequently, the HiBind[®] RNA Mini Column was removed to a new collection tube, and 500 μL VHB Buffer was added in the tube for centrifugation at 13,000 g for 15 s. The filtrate was discarded, and the HiBind[®] RNA Mini Column was removed to a new collection tube. 500 μL Wash Buffer II was added in the tube for centrifugation at 13,000 g for 15 s, and then the filtrate was discarded. This washing step was performed twice. After moving the HiBind[®] RNA Mini Column to a new tube, centrifugation was performed at 13,000 g for 2 min to remove any ethanol. Finally, the HiBind[®] RNA Mini Column was removed to a new tube, and a 20 μL aliquot of pure water was added to the center of the HiBind[®] RNA Mini Column. After performing centrifugation at 13,000 g for 1 min, RNA fragments were collected. The extracted DENV1 RNA was resuspended in 20 μL pure water. After centrifugation of the resuspension, a 130 μL aliquot of 150 mM NaCl-containing 10 mM PBS buffer (pH 6.0) was added to restore the 150 μL initial volume of the DENV sample. Then, 10 μL aliquot of the RNA sample was dropped on the genosensors for 20 min at room temperature for hybridization.

3. Results and Discussion

3.1. Effect of Binary SAM on pDNA Coverage

Most studies directly immobilize thiolated pDNA on gold electrodes via the formation of an Au-S bond for the preparation of genosensors [29,30,32–34]. However, the bases of pDNA have strong non-specific adsorption on the Au surface. MCH of millimolar-scale concentration is commonly used to displace most non-specifically adsorbed pDNA, but some still remained [33]. In this study, the modification of MHA/MCH binary SAM was used as a link for pDNA immobilization to prevent the non-specific adsorption effectively. Figure 1 shows the cyclic voltammograms obtained at the ratio-varied MHA/MCH-modified electrodes. Two cathodic peaks were found in all reductive curves and represented as the desorption behavior of MHA/MCH SAM on the polycrystalline Au substrate. The adsorbing stability of Au-S bond substantially depends on the crystallographic orientation in the order of Au(111) < Au(100) < Au(110) [35]. Therefore, the two reductive peaks at about -0.8 V and -1.1 V were, respectively, attributed to the Au-S desorption in Au (111) face and Au (100) or Au(110) faces. Compared with other MHA/MCH ratios, the first reductive peak obtained at the MHA(0):MCH(1 mM)-modified electrodes was at more negative potential (-0.95 V), resulting from the interaction force between homogeneous MCH molecules stronger than that between MHA and MCH. The coverage of MHA/MCH SAM of 0:1, 0.02:1, 0.04:1 and 0.1:1 ratios calculated by the desorption charge (Q) was, respectively, 9.4 ± 0.3 , 9.4 ± 0.1 , 10.0 ± 0.2 and $10.2 \pm 0.3 \times 10^{-11}$ mol/cm² ($n = 4$). The result showed that the SAM coverage was positively proportional to the total concentration of MHA/MCH mixture.

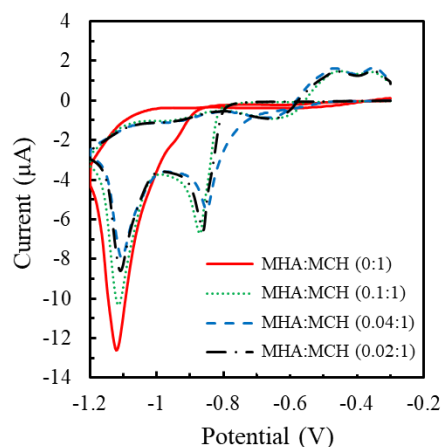


Figure 1. Cyclic voltammograms respectively obtained from the MHA/MCH-modified electrodes with the concentration (mM) ratios of 0:1 (red solid line), 0.1:1 (green dotted line), 0.04:1 (blue dashed line) and 0.02:1 (black dot-dashed line) in 0.5 mM NaOH from -0.3 V to -1.2 V with the scan rate of 100 mV/s.

Furthermore, EIS was used to estimate the MHA ratio in the binary SAM due to the repulsive force between the negatively charged COOH group of MHA and the $\text{Fe}(\text{CN})_6^{3-/4-}$ [31]. Figure 2a shows the Nyquist plots obtained at bare, 1 mM MCH, 1 mM MHA and ratio-varied MHA/MCH modified electrodes. The impedance spectra measured at the MCH-modified electrode (curve ii of Figure 2a) exhibited a significant linear region, implying the diffusion-controlled behavior of the $\text{Fe}(\text{CN})_6^{3-/4-}$ mediator at the lower frequencies, and a semicircle region, implying the kinetics-controlled behavior [31]. The radius of the semicircle is related to the R_{et} of mediator in the electrode/electrolyte interface. The radius of the semicircle obtained at the binary SAM-modified electrodes increased with the increasing MHA ratio, attributed to the electrostatically repulsive force of COOH group of MHA molecules [31]. Furthermore, the semicircle radius of the impedimetric plot of the 1 mM MCH-modified electrode was much smaller than the bare electrode, implying that the hydrophilic OH group of MCH can significantly reduce the R_{et} . It is worth noting that the impedimetric plots

only exist in the semicircle part when the ratio of MHA to MCH is larger than 0.04:1, implying that the higher density of MHA makes the concentration gradient of the mediator harder to produce a difference between the bulk solution and the electrode surface.

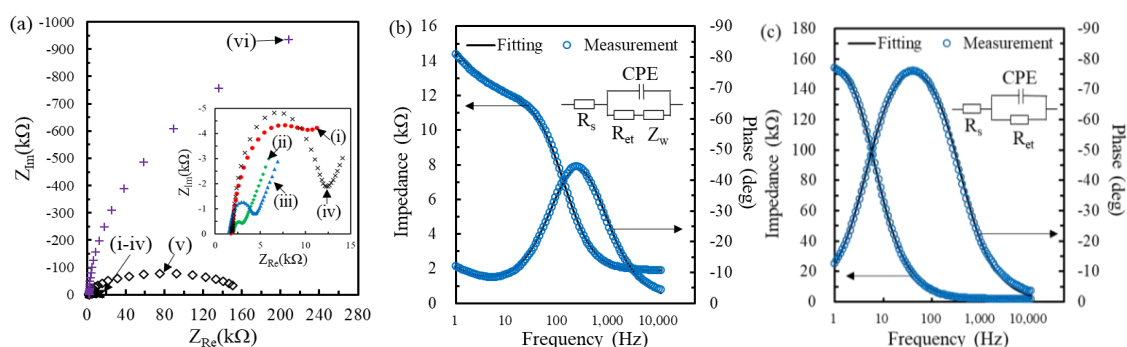


Figure 2. (a) Nyquist plots obtained at the Au electrode in a 26 mM N-[Tris(hydroxymethyl)methyl]-2-aminoethanesulfonic acid (TES) buffer containing 1 mM equimolar $\text{Fe}(\text{CN})_6^{3-/4-}$ before and after the modification of MHA:MCH (mM) mixture of 0:1 (ii), 0.02:1 (iii), 0.04:1 (iv), 0.1:1 (v) or 1:0 (vi). Bode plots measured at the MHA (0.04 mM)/MCH(1 mM) (b) and MHA (0.1 mM)/MCH(1 mM) (c)-modified electrodes. Inset of (b) and (c) respectively shows the diagram of modified Randles equivalent circuit and 1R//C circuit.

Two kinds of equivalent circuits, a modified Randles model (inset of Figure 2b) and a 1R//C model (inset of Figure 2c), were used to simulate the impedimetric results with and without the diffusion-controlled region, respectively. The equivalent circuit of modified Randles model consists of four elements: the solution resistance (R_s), the Warburg impedance (Z_w), the constant phase element (CPE) of electrical double layer and R_{et} . Because the double layer is not an ideal capacitor (C_{dl}) due to the Faradic current leakage of $\text{Fe}(\text{CN})_6^{3-/4-}$ mediator, CPE was used to replace C_{dl} in the equivalent circuit, especially for the surface-modified electrodes [34]. The impedance of the CPE can be presented as $Z_{CPE}(\omega) = Z_0(j\omega)^{-\alpha}$, where Z_0 is a constant, j is an imaginary number, ω is the angular frequency, and $0 < \alpha < 1$. When α is closer to 1, the CPE becomes more capacitive. When the impedimetric spectrum only contains the kinetics-controlled part, the 1R//C model is used to explain the EIS behavior, such as MHA(0.1 mM)/MCH(1 mM)-modified electrodes, which consist of one resistor (R_s) in series with one parallel circuit comprising a resistor (R_{et}) and a capacitor (CPE). Figure 2b,c, respectively, shows the Bode plots of experimental data measured at the MHA(0.04 mM)/MCH(1 mM)/Au electrode and the MHA(0.1 mM)/MCH(1 mM)/Au electrode, and the corresponding computer fitting using the modified Randles and the 1R//C equivalent circuit. The fitting results show good consistency with the experimental measurement with a mean error of less than 0.2% and a maximum error of 2.2% for all fitting data. After the fitting of equivalent circuits, the R_{et} value obtained at bare, MCH(1 mM), MHA(0.02 mM)/MCH(1 mM), MHA(0.04 mM)/MCH(1 mM), MHA(0.1 mM)/MCH(1 mM) and MHA(1 mM) modified electrodes was, respectively, 13 ± 0 kΩ, 1 ± 0 kΩ, 2 ± 0 kΩ, 10 ± 0 kΩ, 156 ± 1 kΩ and 5578 ± 164 kΩ ($n = 3$). The smallest R_{et} value obtained at the 1 mM MCH-modified electrodes is attributed to the good hydrophilicity of MCH hydroxyl group. Moreover, the R_{et} value actually increased with the increasing ratio of MHA in the binary SAMs due to the repulsively electrostatic force from the COO^- group of MHA.

The MHA ratio of SAM could determine the density of immobilized pDNA. The coulometric method was used to measure the pDNA density via the reductive charge of RuHex adsorbed on the phosphate group of pDNA, after immobilization of pDNA on the MHA-activated surface. Figure 3 shows the chronocoulometric curves measured from the different pDNA/MHA/MCH/Au electrodes in the absence and presence of RuHex. Here, the denotation of MCH concentration is omitted for a concise reading because the concentration, 1 mM, of MCH used for all MHA/MCH modification was the same. The fitting range for the 1 mM MHA SAM was from $0.2 \text{ s}^{1/2}$ to $0.7 \text{ s}^{1/2}$, and for the all MHA/MCH binary

SAM was from $0.1 \text{ s}^{1/2}$ to $0.4 \text{ s}^{1/2}$. The intercepts of fitting line at $t = 0$ obtained in the RuHex-containing buffer and the Tris buffer, respectively, were used for the calculation of Γ_0 [32]. The Γ_0 measured on the pDNA/MHA(1 mM)/Au, the pDNA/MHA(0.1 mM)/MCH/Au, pDNA/MHA(0.04 mM)/MCH/Au and the pDNA/MHA(0.02 mM)/MCH/Au electrodes was, respectively, 175.8 ± 3.4 , 16.1 ± 6.1 , 4.5 ± 0.4 and $3.2 \pm 0.5 \times 10^{11} \text{ pDNA/cm}^2$ ($n = 3$) and the interval between two adjacent pDNA molecules on the electrodes was respectively calculated as 2.4 nm, 7.9 nm, 14.9 nm and 17.7 nm by assuming a homogeneous distribution of pDNA on the SAM surface. The result shows that the Γ_0 of immobilized pDNA is positively correlated to the MHA ratio of MHA/MCH SAMs. Nevertheless, the 2.4 nm wide interval between two adjacent pDNA molecules on the pDNA/MHA(1 mM)/Au genosensors is adverse to the tDNA hybridization because the diameter of double-stranded DNA is 2 nm. Moreover, the electrostatically repulsive force of the phosphate group in the hybridized DNA backbone may hinder the hybridization of another suspended tDNA. The thickness ($=3.04/(IS^{0.5}) \text{ \AA}$) of the electric double layer is calculated as 0.7 nm with 190 mM IS in the 150 mM NaCl-containing 10 mM phosphate buffer (pH 7.0) solution. Steel et al. also demonstrated that the pDNA density greater than $4 \times 10^{12} \text{ pDNA/cm}^2$ significantly reduced the hybridizing efficiency of complementary tDNA [32]. Therefore, the modification of MHA (1 mM) is not used to construct the genosensors.

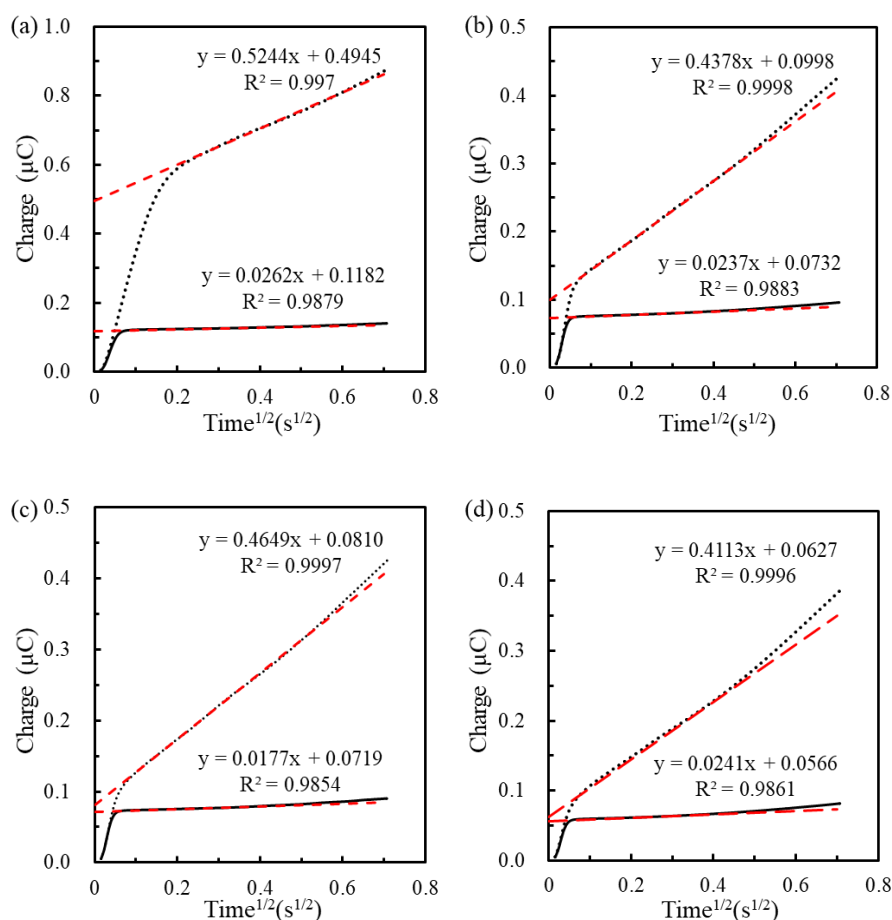


Figure 3. Chronocoulometric curves obtained in 10 mM tris(hydroxymethyl)aminomethane (Tris) buffer (solid line) and 50 μM RuHex-containing 10 mM Tris buffer (dotted line) by applying a step potential from 0.1 V to -0.4 V for 500 ms on the pDNA/MHA(1 mM)/Au electrode (a), the pDNA/MHA(0.1 mM)/MCH(1 mM)/Au electrode (b), the pDNA/MHA(0.04 mM)/MCH(1 mM)/Au electrode (c) and the pDNA/MHA(0.02 mM)/MCH(1 mM)/Au electrode (d). The red dash lines show the fits from the raw data.

3.2. Effect of pDNA Density on Hybridization of Length-Varied tDNA

The interval between the immobilized pDNA molecules could affect the hybridization degree [32]. Figures 4 and 5 show the impedimetric spectra obtained at the genosensors modified with the MHA/MCH SAM of different ratios for the hybridization of 20mtDNA and 160mtDNA, respectively. The results presented that the radius of all semicircle increased with the tDNA hybridization. After simulation of the 1R//C model for the genosensors modified by MHA(0.1 mM)/MCH and MHA(0.04 mM)/MCH, and the modified Randles model for the genosensors modified by MHA(0.02 mM)/MCH, the R_{et} increment ($\Delta R_{et} = R_{et-Tdna} - R_{et-pDNA}$) and the ΔR_{et} ratio (%) ($= \Delta R_{et}/R_{et-pDNA} \times 100$) of genosensors after the hybridization of 1 pM and 1 nM tDNA are compared in Table 2. The ΔR_{et} obtained from the three kinds of MHA/MCH genosensors increased with the tDNA concentration, and the ΔR_{et} obtained at the denser pDNA-immobilized-genosensors increased more significantly. Moreover, the ΔR_{et} obtained at the 160mtDNA-hybridized genosensors was much larger than that obtained at the 20mtDNA-hybridized genosensors, resulting from the steric and repulsive hindrance of the 140-mer electrode side overhang of 160mtDNA from the permeation of $Fe(CN)_6^{3-/4-}$ to the electrode. Riedel et al. found a similar phenomenon when using a 10-mer electrode side overhang tDNA to obtain the larger ΔR_{et} ratio than a 5-mer electrode side overhang [30].

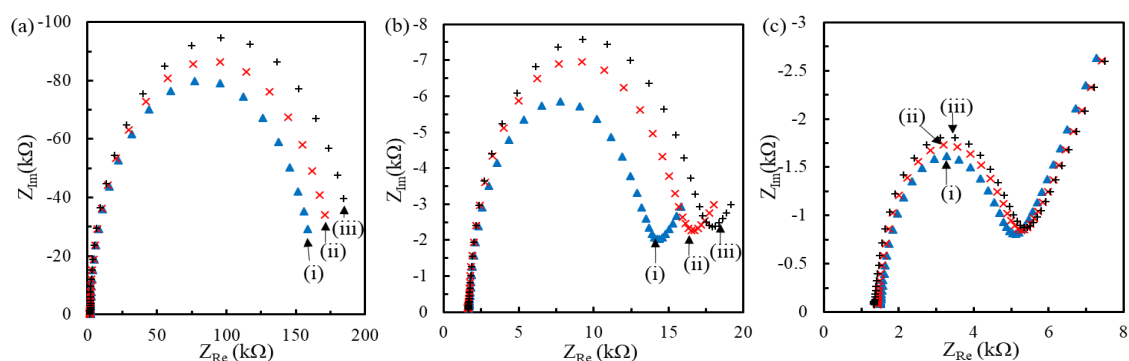


Figure 4. Nyquist plots obtained at the pDNA/MHA/MCH/Au genosensors (i) with the MHA:MCH layer of 0.1:1 (a), 0.04:1 (b) and 0.02:1 ratio (c) followed by the hybridization of 1 pM (ii) and 1 nM (iii) 20mtDNA. The buffer for electrochemical impedance spectroscopy (EIS) measurement is the 26 mM TES buffer containing 1 mM equimolar $Fe(CN)_6^{3-/4-}$.

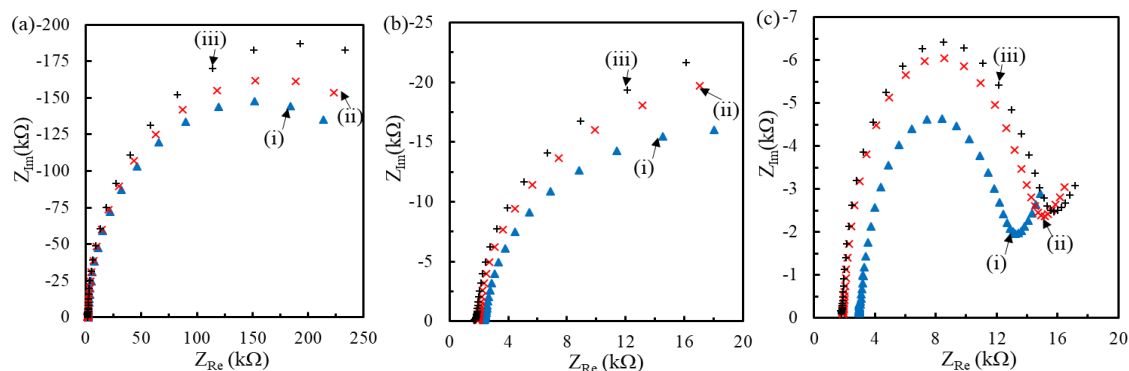


Figure 5. Nyquist plots obtained at the pDNA/MHA/MCH/Au genosensors (i) with the MHA:MCH layer of 0.1:1 (a), 0.04:1 (b) and 0.02:1 ratio (c) followed by the hybridization of 1 pM (ii) and 1 nM (iii) 160mtDNA. The buffer for EIS measurement is the same with Figure 4.

Table 2. Comparison of the R_{et} Increment ($\Delta R_{et} = R_{et-tDNA} - R_{et-pDNA}$) and the ΔR_{et} ratio (%) ($= (\Delta R_{et}/R_{et-pDNA}) \times 100$) Measured from Different pDNA/MHA/MCH/Au Genosensors after Hybridization with 20mtDNA and 160mtDNA. Each Value is Calculated from Three Individual Genosensors.

Ratio of MHA: MCH	20mtDNA				160mtDNA			
	ΔR_{et} (k Ω)		ΔR_{et} Ratio (%)		ΔR_{et} (k Ω)		ΔR_{et} Ratio (%)	
	1 pM	1 nM	1 pM	1 nM	1 pM	1 nM	1 pM	1 nM
0.10:1	18.3 \pm 4.3	32.2 \pm 7.1	10.1 \pm 1.9	17.8 \pm 5.5	63.7 \pm 42.2	120.2 \pm 47.4	16.2 \pm 11.2	30.4 \pm 12.5
0.04:1	1.8 \pm 0.7	3.1 \pm 0.9	17.0 \pm 4.0	30.0 \pm 4.3	11.0 \pm 2.2	17.8 \pm 2.8	32.9 \pm 7.1	53.0 \pm 9.3
0.02:1	0.3 \pm 0.1	0.4 \pm 0.1	9.3 \pm 1.8	13.8 \pm 1.4	2.8 \pm 0.30	3.2 \pm 0.2	30.2 \pm 3.6	35.1 \pm 1.4

Compared to the ΔR_{et} , ΔR_{et} ratio is more often used to compare the ΔR_{et} increment between different modified electrodes by normalizing the initial impedimetric status of pre-hybridized genosensors [29,30]. It is worth noting that the ΔR_{et} ratio obtained at the MHA(0.04 mM)/MCH-modified genosensors was larger than that obtained at the MHA(0.1 mM)/MCH- and MHA(0.02 mM)/MCH-modified genosensors. Moreover, the ΔR_{et} ratio of 160mtDNA hybridization was much larger than that of 20mtDNA hybridization. The results indicated that the pDNA density of MHA(0.04 mM)/MCH-modified genosensors was more effective for the hybridization of 160mtDNA than other MHA/MCH-modified genosensors. The smaller interval between the pDNA molecules of the MHA(0.1 mM)/MCH-modified genosensors was adverse to the hybridization of long electrode side overhangs of 160mtDNA. Although the larger interval between the pDNA molecules of the MHA(0.02 mM)/MCH-modified genosensors was beneficial to the hybridization of 160mtDNA, the reduced pDNA density produced lower ΔR_{et} ratio than that obtained at the other MHA/MCH-modified genosensors and was easier to reach saturated hybridization. The increment of ΔR_{et} ratio from 1 pM to 1 nM 160mtDNA measured at the MHA(0.02 mM)/MCH-modified genosensors was only 4.9%, which was smaller than that (20.2%) measured at the MHA(0.04 mM)/MCH-modified genosensors. The results suggested that the MHA(0.04 mM)/MCH-modified genosensors was more suitable for the hybridization of extracted DENV1 RNA due to the similar electrode side overhangs with the 160mtDNA.

3.3. Sensing Properties of Genosensors for Extracted RNA

The MHA(0.04 mM)/MCH-modified genosensors were used to measure the extracted RNA samples. Figure 6a shows the Nyquist plots obtained at the pDNA/MHA(0.04 mM)/MCH-modified genosensors followed by time-lapse hybridization of RNA samples extracted from 10^4 PFU/mL DENV1. The increasing radius of semicircle suggested the increase of R_{et} due to the extracted RNA hybridization. Figure 6b shows the time-lapse change of ΔR_{et} ratio ($n = 3$) corresponding to the fitting result of Figure 6a. The ΔR_{et} ratio increased with time. The ΔR_{et} ratio ($142.1 \pm 3.1\%$) at 20 min had smaller relative standard deviation (RSD) of 2.2%, implying better reproducibility, and the increment of ΔR_{et} ratio slowed down after 20 min hybridization. Therefore, 20 min hybridization for each concentration was used to test the calibration curve. Furthermore, the ΔR_{et} ratio (142.1%) of 20 min hybridization, compared to the R_{et} value (8.7 ± 0.8 k Ω) of pre-hybridized genosensors with the background noise of 8.7% RSD, was significantly larger than the background noise.

Figure 7a presents the Nyquist plots for the genosensors before and after hybridizing the RNA samples extracted from the concentration-varied DENV1. After fitting, Figure 7b shows the corresponding calibration curve obtained from three individual genosensors. The result presented that the genosensors had a good linearity ($R = 0.9960$) in the range of 10^2 – 10^5 PFU/mL with a regressive equation of ΔR_{et} ratio = $33.3 \log[\text{DENV}] - 43.1$ and saturated at the 10^5 PFU/mL. The R_{et} value of pre-hybridized genosensors was 8.5 ± 0.2 k Ω , implying the calculated limit of detection (LOD) was about 20 PFU/mL ($S/N > 3$). Generally, 1 PFU of DENV is equivalent to 600–1000 copies of virus particles in Dr. Perng's laboratory, which depends on the virus strains, culture conditions and the stored time of the virus [36,37]. The 20 PFU/mL LOD is equal to 20–33 aM RNA copies, which is much lower than that (1 fM extracted RNA of DENV2) of the EIS-based pDNA/SiO₂@APTES-GO/Pt genosensors [16]. The low LOD was attributed to the very long solution side overhangs and electrode side overhangs of

hybridized RNA to hinder the permeation of mediator to the electrode surface, significantly increasing R_{et} . The ΔR_{et} ratio of 10^4 PFU/mL obtained in the calibration curve was different from that presented in the time-lapse hybridization, partly attributed to the different amount of complementary fragments of extracted RNA and the different hybridizing procedures. As expected, it was difficult to obtain the same copy number of complementary fragments in each extracting procedure. Furthermore, in the previous study [16] the genosensors required a 5 h hybridization incubation and the EIS signal still could not distinguish extracted DENV2 RNA concentrations between 1 fM and 10 pM after hybridization. In contrast, the pDNA/MCH(0.04 mM)/MCH-modified genosensors directly detected the extracted RNA of lower concentration (20 aM) in shorter hybridization time (20 min). According to the reviews by Anusha et al. [25] and Darwish et al. [38], while the electrochemical immunoassays for the detection of DENV NS1, envelope protein and particles can have extremely low LOD down to less than 1 PFU/mL, it remains difficult to distinguish the serotypes of DENV.

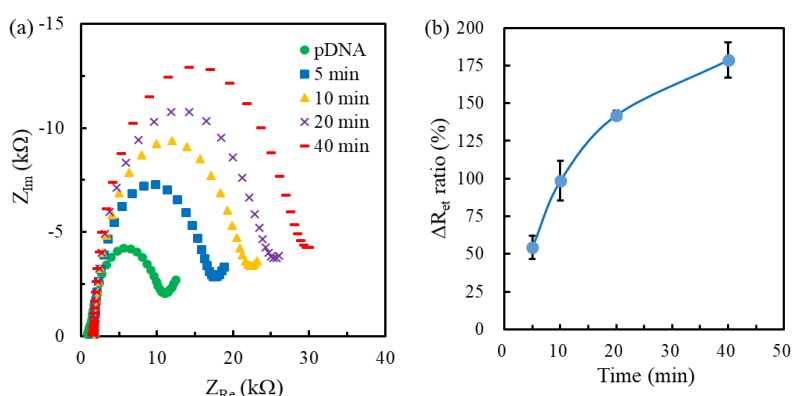


Figure 6. (a) Nyquist plots obtained at the pDNA/MHA(0.04 mM)/MCH(1 mM)/Au genosensors continuously hybridized with the extracted RNA fragments of 10^4 plaque forming units (PFU)/mL dengue virus (DENV1) for different length of times. (b) The corresponding time-lapse ΔR_{et} ratio.

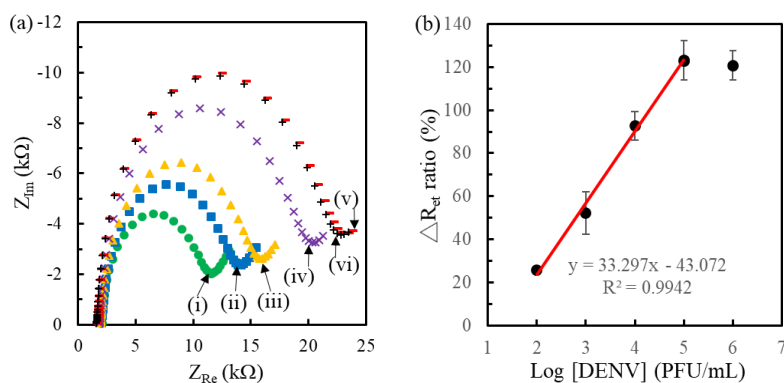


Figure 7. (a) Nyquist plots obtained at the pDNA/MHA(0.04 mM)/MCH(1 mM)/Au genosensors (i) followed by the 20 min hybridization of RNA fragments extracted from 10^2 (ii), 10^3 (iii), 10^4 (iv), 10^5 (v) and 10^6 (vi) PFU/mL DENV1. (b) The corresponding calibration curve of the genosensors ($n = 3$).

The selectivity test of genosensors is shown in Figure 8. The hybridization efficiency of the extracted RNA samples of each DENV serotype were respectively measured by three individual genosensors. The ΔR_{et} ratio ($56.4 \pm 7.9\%$) for DENV1 is significantly larger than that for DENV2 ($11.4 \pm 3.4\%$), DENV3 ($17.4 \pm 2.3\%$) and DENV4 ($14.7 \pm 2.9\%$) ($p < 0.05$ by student t -test). Moreover, the ΔR_{et} ratio value for the mixture of DENV1+2, DENV1+3 and DENV1+4 was, respectively, $58.4 \pm 4.4\%$, $60.3 \pm 5.0\%$ and $57.8 \pm 2.0\%$. The calculated selectivity (= DENV1/DENV mixture) was in the range of 93.5% to 97.6%, indicating the good selectivity of the self-designed pDNA-immobilized genosensors

to DENV1. Furthermore, real-time PCR method was used to identify the specificity of self-designed pDNA as shown in Figure 9. The performance of real-time PCR is according to the handbook of KAPA SYBR® FAST qPCR Master Mix (2X) kit. The self-designed pDNA was used as a specific backward primer, and the sequence of 5'-GGTTAGAGGAGACCCCTCCC-3' was used as a universal forward primer, which is suitable for all DENVs. The result shows that the threshold cycle for DENV1 is much smaller than that for DENV2, 3 and 4, implying that the self-designed pDNA is very specific to DENV1. Moreover, Table 3 compares this study with previous electrochemical genosensors for the DENV detection. Most DENV genosensors detected synthesized DNA [15,18–20,39] fragments and nucleic acid amplicons [26,39–41]. Although Chen et al. could obtain as low as 2 PFU/mL LOD, the nucleic acid amplification was necessary [40]. Except for Jin's study [16] and this study, there are few studies to directly detect the extracted RNA without the process of nucleic acid amplification. Moreover, the pDNA/MHA(0.04 mM)/MCH(1 mM)/Au genosensors have better sensing properties than Jin's sensor.

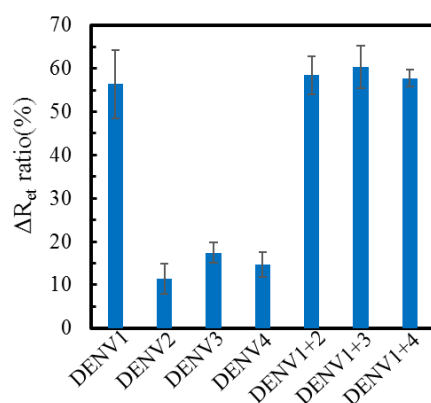


Figure 8. The serotypic selectivity test for the RNA samples extracted from four serotypes of 10^4 PFU/mL DENV ($n = 3$).

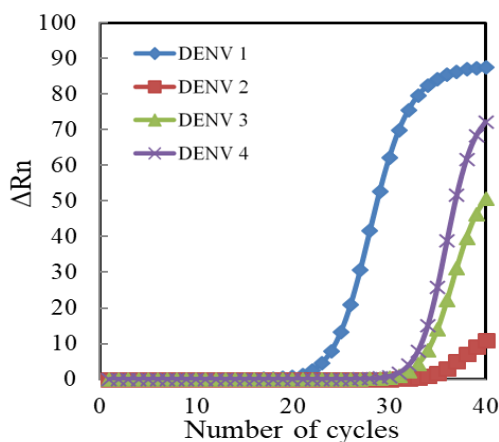


Figure 9. Fluorescence chart produced by real-time polymerase chain reaction (PCR) assay for the specificity of self-designed pDNA for four serotypes of 10^6 PFU/mL DENV.

Table 3. Comparison of the Sensing Properties of Different Genosensors for the Detection of DENV.

Sensing Interface	Method/Target	Dynamic Range	LOD	Ref.
pDNA2-liposome/biotin-pDNA1-SMB	Fluorescence/synthetic DNA and RNA amplicon	0.125 nM–50 pM	0.125 nM	[39]
SH-pDNA-AuNP	QCM/PCR 130mtDNA amplicon	2×10^0 – 2×10^6 PFU/mL	2 PFU/mL	[40]
pDNA/IEM	I-V curve/RT-PCR DNA amplicon	–	0.17 aM	[41]
NH ₂ -pDNA/APS/Pt/AAO	EIS or DPV/synthetic 30mtDNA	1 pM–1 μ M	2.7 pM	[15]
pDNA/PGE	DPV/synthetic 22mtDNA	10–100 nM	3.1 nM	[18]
NH ₂ -pDNA/chitosan/ZnO/Pt-Pd/FTO	CV/synthetic 35mtDNA	1–100 μ M	43 μ M	[19]
NH ₂ -pDNA/MPA/Mn ₂ O ₃ nanofiber/GCE	EIS or DPV/synthetic consensus dengue primer	1 aM–1 μ M	0.12 aM	[20]
ITO	LSV/pDNA-RNA amplicon mixture	–	2 amol	[26]
pDNA/SiO ₂ @APTES-GO/Pt	EIS/extracted RNA	–	1 fM	[16]
NH ₂ -pDNA/MHA/MCH/Au	EIS/extracted RNA	10^2 – 10^5 PFU/mL	20 PFU/mL (~20 aM)	This work

AAO: anodic aluminum oxide, APS: 3-aminopropyltrimethoxysilane, DPV: differential pulse voltammetry, FTO: fluorine doped tin oxide, IEM: ion-exchange nanomembrane sensor, I-V: current-voltage, LSV: linear sweep voltammetry, SMB: streptavidin magnetic bead, MPA: mercaptopropionic acid, PGE: pencil graphite electrode, QCM: quartz crystal microbalance, SPR: surface plasmon resonance, LOD: limit of detection.

4. Conclusions

The ratio-varied MHA/MCH binary SAM can be used as a link to control the density of immobilized pDNA. In particular, the pDNA/MHA(0.04 mM)/MCH-modified genosensors improved the hybridization efficiency for 160 mtDNA having 140-mer electrode side overhangs via the EIS analysis. The genosensors designed in this study could detect extracted DENV1 RNA after 20 min hybridization with a low LOD of 20 PFU/mL, good detection linearity from 10^2 to 10^5 PFU/mL and good selectivity for DENV1. This study demonstrates that the combination of well-controlled pDNA density and the self-designed pDNA sequence capable of reducing the electrode side overhang length of extracted RNA makes the detection of extracted DENV1 RNA feasible. As expected, this method has great promise to construct label-free EIS-based genosensors for the optimal hybridization of extracted nucleic acids without the process of nucleic acid amplification.

Author Contributions: C.-C.W.: Writing-original draft, Methodology, Conceptualization, Validation, Writing-review & editing. H.-Y.Y.: Methodology, Conceptualization, Validation, Formal analysis. L.-T.L.: Methodology, Conceptualization, Validation, Formal analysis. G.-C.P.: Resources, Validation. C.-R.L.: Conceptualization, Writing-review & editing. S.-J.W.: Conceptualization, Writing-review & editing, Funding acquisition. All authors have read and agreed to the published version of the manuscript.

Funding: This research was financially supported by the Henry M. Jackson Foundation for the Advancement of Military Medicine grant number [895748]; the Naval Medical Research Center (NMRC) grant number [N3239818P0305]; the Ministry of Science and Technology of Taiwan grant number [MOST107-2313-B-005-006-MY3], and the “Innovation and Development Center of Sustainable Agriculture” from The Featured Areas Research Center Program within the framework of the Higher Education Sprout Project by the Ministry of Education in Taiwan. This work was partly funded by the Military Infectious Diseases Research Program grant number [L0427_16_NM] and supported by NMRC Work Unit Number A1223.

Acknowledgments: We thank Hua-Wei Chen for his help in reviewing the manuscript.

Conflicts of Interest: The authors declare no conflict of interest.

Disclaimer: The views expressed in this article are those of the authors, and do not necessarily reflect the official policy or position of the Department of the Navy, the Department of Defense, or the US Government. Shuenn-Jue Wu is a U.S. government employee. This work was prepared as part of her official duties. Title 17 U.S.C. § 105 provides that ‘Copyright protection under this title is not available for any work of the United States Government.’ Title 17 U.S.C. § 101 defines a U.S. Government work as a work prepared by military service members or employees of the U.S. Government as part of those persons’ official duties. Cheng-Rei Lee was employed by the Henry M. Jackson Foundation for the Advancement of Military Medicine and was funded to do this work by the U.S. Government.

References

1. Fernandes, J.N.; Moise, I.K.; Maranto, G.L.; Beier, J.C. Revamping Mosquito-borne Disease Control to Tackle Future Threats. *Trends Parasitol.* **2018**, *34*, 359–368. [[CrossRef](#)] [[PubMed](#)]
2. Chastel, C. Eventual role of asymptomatic cases of dengue for the introduction and spread of dengue viruses in non-endemic regions. *Front Physiol.* **2012**, *3*, 70. [[CrossRef](#)] [[PubMed](#)]
3. Ratnam, I.; Leder, K.; Black, J.; Torresi, J. Dengue fever and international travel. *J. Travel Med.* **2013**, *20*, 384–393. [[CrossRef](#)] [[PubMed](#)]
4. Weaver, S.C. Urbanization and geographic expansion of zoonotic arboviral diseases: Mechanisms and potential strategies for prevention. *Trends Microbiol.* **2013**, *21*, 360–363. [[CrossRef](#)]
5. Malavige, G.N.; Fernando, S.; Fernando, D.J.; Seneviratne, S.L. Dengue viral infections. *Postgrad. Med. J.* **2004**, *80*, 588–601. [[CrossRef](#)] [[PubMed](#)]
6. Peeling, R.W.; Artsob, H.; Pelegrino, J.L.; Buchy, P.; Cardoso, M.J.; Devi, S.; Enria, D.A.; Farrar, J.; Gubler, D.J.; Guzman, M.G.; et al. Evaluation of diagnostic tests: Dengue. *Nat. Rev. Microbiol.* **2010**, *8*, S30–S38. [[CrossRef](#)]
7. Bhatt, S.; Gething, P.W.; Brady, O.J.; Messina, J.P.; Farlow, A.W.; Moyes, C.L.; Drake, J.M.; Brownstein, J.S.; Hoen, A.G.; Sankoh, O.; et al. The global distribution and burden of dengue. *Nature* **2013**, *496*, 504–507. [[CrossRef](#)]
8. Lo, Y.C.; Perng, G.C. Novel concept on antiviral strategies to dengue. *Curr. Opin. Virol.* **2016**, *18*, 97–108. [[CrossRef](#)]
9. Iswardy, E.; Tsai, T.C.; Cheng, I.F.; Ho, T.C.; Perng, G.C.; Chang, H.C. A bead-based immunofluorescence-assay on a microfluidic dielectrophoresis platform for rapid dengue virus detection. *Biosens. Bioelectron.* **2017**, *95*, 174–180. [[CrossRef](#)]
10. Lim, J.M.; Kim, J.H.; Ryu, M.Y.; Cho, C.H.; Park, T.J.; Park, J.P. An electrochemical peptide sensor for detection of dengue fever biomarker NS1. *Anal. Chim. Acta* **2018**, *1026*, 109–116. [[CrossRef](#)]
11. Nawaz, M.H.; Hayat, A.; Catanante, G.; Latif, U.; Marty, J.L. Development of a portable and disposable NS1 based electrochemical immunosensor for early diagnosis of dengue virus. *Anal. Chim. Acta* **2018**, *1026*, 1–7. [[CrossRef](#)] [[PubMed](#)]
12. Basso, C.R.; Crulhas, B.P.; Magro, M.; Vianello, F.; Pedrosa, V.A. A new immunoassay of hybrid nanomater conjugated to aptamers for the detection of dengue virus. *Talanta* **2019**, *197*, 482–490. [[CrossRef](#)] [[PubMed](#)]
13. Cheng, M.S.; Ho, J.S.; Tan, C.H.; Wong, J.P.; Ng, L.C.; Toh, C.S. Development of an electrochemical membrane-based nanobiosensor for ultrasensitive detection of dengue virus. *Anal. Chim. Acta* **2012**, *725*, 74–80. [[CrossRef](#)] [[PubMed](#)]
14. Vickers, I.; Harvey, K.; Nelson, K.; Brown, M.; Bullock-DuCassee, M.; Lindo, J. Evaluation of OneStep Dengue NS1 RapiDip InstaTest and OneStep Dengue Fever IgG/IgM RapiCard InstaTest during the course of a dengue type 1 epidemic. *Diagn. Microbiol. Infect. Dis.* **2017**, *89*, 271–275. [[CrossRef](#)] [[PubMed](#)]
15. Deng, J.; Toh, C.S. Impedimetric DNA biosensor based on a nanoporous alumina membrane for the detection of the specific oligonucleotide sequence of dengue virus. *Sensors* **2013**, *13*, 7774–7785. [[CrossRef](#)] [[PubMed](#)]
16. Jin, S.-A.; Poudyal, S.; Marinero, E.E.; Kuhn, R.J.; Stanciu, L.A. Impedimetric Dengue Biosensor based on Functionalized Graphene Oxide Wrapped Silica Particles. *Electrochim. Acta* **2016**, *194*, 422–430. [[CrossRef](#)]
17. Odeh, A.A.; Al-Douri, Y.; Voon, C.H.; Ayub, R.M.; Gopinath, S.C.B.; Odeh, R.A.; Ameri, M.; Bouhemadou, A. A needle-like Cu₂CdSnS₄ alloy nanostructure-based integrated electrochemical biosensor for detecting the DNA of Dengue serotype 2. *Microchim. Acta* **2017**, *184*, 2211–2218. [[CrossRef](#)]
18. Oliveira, N.; Souza, E.; Ferreira, D.; Zanforlin, D.; Bezerra, W.; Borba, M.A.; Arruda, M.; Lopes, K.; Nascimento, G.; Martins, D.; et al. A sensitive and selective label-free electrochemical DNA biosensor for the detection of specific dengue virus serotype 3 sequences. *Sensors* **2015**, *15*, 15562–15577. [[CrossRef](#)]
19. Singhal, C.; Pundir, C.S.; Narang, J. A genosensor for detection of consensus DNA sequence of Dengue virus using ZnO/Pt-Pd nanocomposites. *Biosens. Bioelectron.* **2017**, *97*, 75–82. [[CrossRef](#)]
20. Tripathy, S.; Vanjari, S.R.K.; Singh, V.; Swaminathan, S.; Singh, S.G. Electrospun manganese (III) oxide nanofiber based electrochemical DNA-nanobiosensor for zeptomolar detection of dengue consensus primer. *Biosens. Bioelectron.* **2017**, *90*, 378–387. [[CrossRef](#)]
21. Sharp, T.M.; Perez-Padilla, J.; Waterman, S.H. Travel-Related Infectious Diseases. 2019. Available online: <https://wwwnc.cdc.gov/travel/yellowbook/2020/travel-related-infectious-diseases/dengue> (accessed on 26 October 2019).

22. Boonnak, K.; Slike, B.M.; Burgess, T.H.; Mason, R.M.; Wu, S.J.; Sun, P.; Porter, K.; Rudiman, I.F.; Yuwono, D.; Puthavathana, P.; et al. Role of dendritic cells in antibody-dependent enhancement of dengue virus infection. *J. Virol.* **2008**, *82*, 3939–3951. [[CrossRef](#)]
23. Balsitis, S.J.; Williams, K.L.; Lachica, R.; Flores, D.; Kyle, J.L.; Mehlhop, E.; Johnson, S.; Diamond, M.S.; Beatty, P.R.; Harris, E. Lethal antibody enhancement of dengue disease in mice is prevented by Fc modification. *PLoS Pathog.* **2010**, *6*, e1000790. [[CrossRef](#)] [[PubMed](#)]
24. Darwish, N.T.; Sekaran, S.D.; Khor, S.M. Point-of-care tests: A review of advances in the emerging diagnostic tools for dengue virus infection. *Sens. Actuator B-Chem.* **2018**, *255*, 3316–3331. [[CrossRef](#)]
25. Anusha, J.R.; Kim, B.C.; Yu, K.H.; Raj, C.J. Electrochemical biosensing of mosquito-borne viral disease, dengue: A review. *Biosens. Bioelectron.* **2019**, *142*, 111511. [[CrossRef](#)] [[PubMed](#)]
26. Cui, J.; Gao, L.; Chen, S.; Huang, Z.; Wang, X. Electrochemical voltammetric behaviors of synthetic dengue virus RNAs at ITO sensing electrode. *J. Electroanal. Chem.* **2019**, *851*, 113463. [[CrossRef](#)]
27. Lynch, C.A., III; Foguel, M.V.; Reed, A.J.; Balcarcel, A.M.; Calvo-Marzal, P.; Gerasimova, Y.V.; Chumbimuni-Torres, K.Y. Selective determination of isothermally amplified Zika virus RNA using a universal DNA-hairpin probe in less than 1 h. *Anal. Chem.* **2019**, *91*, 13458–13464. [[CrossRef](#)] [[PubMed](#)]
28. Mills, D.M.; Martin, C.P.; Armas, S.M.; Calvo-Marzal, P.; Kolpashchikov, D.M.; Chumbimuni-Torres, K.Y. A universal and label-free impedimetric biosensing platform for discrimination of single nucleotide substitutions in long nucleic acid strands. *Biosens. Bioelectron.* **2018**, *100*, 35–42. [[CrossRef](#)]
29. Corrigan, D.K.; Schulze, H.; McDermott, R.A.; Schmäser, I.; Henihan, G.; Henry, J.B.; Bachmann, T.T.; Mount, A.R. Improving electrochemical biosensor performance by understanding the influence of target DNA length on assay sensitivity. *J. Electroanal. Chem.* **2014**, *732*, 25–29. [[CrossRef](#)]
30. Riedel, M.; Kartchemnik, J.; Schonung, M.J.; Lisdat, F. Impedimetric DNA detection—steps forward to sensorial application. *Anal. Chem.* **2014**, *86*, 7867–7874. [[CrossRef](#)]
31. Ding, S.-J.; Chang, B.-W.; Wu, C.-C.; Lai, M.-F.; Chang, H.-C. Impedance spectral studies of self-assembly of alkanethiols with different chain lengths using different immobilization strategies on Au electrodes. *Anal. Chim. Acta* **2005**, *554*, 43–51. [[CrossRef](#)]
32. Steel, A.B.; Herne, T.M.; Tarlov, M.J. Electrochemical Quantitation of DNA Immobilized on Gold. *Anal. Chem.* **1998**, *70*, 4670–4677. [[CrossRef](#)] [[PubMed](#)]
33. Herne, T.M.; Tarlov, M.J. Characterization of DNA Probes Immobilized on Gold Surfaces. *J. Am. Chem. Soc.* **1997**, *119*, 8916–8920. [[CrossRef](#)]
34. Wu, C.-C.; Huang, W.-C.; Hu, C.-C. An ultrasensitive label-free electrochemical impedimetric DNA biosensing chip integrated with a DC-biased AC electroosmotic vortex. *Sens. Actuator B-Chem.* **2015**, *209*, 61–68. [[CrossRef](#)]
35. Arihara, K.; Ariga, T.; Takashima, N.; Arihara, K.; Okajima, T.; Kitamura, F.; Tokuda, K.; Ohsaka, T. Multiple voltammetric waves for reductive desorption of cysteine and 4-mercaptobenzoic acid monolayers self-assembled on gold substrates. *Phys. Chem. Chem. Phys.* **2003**, *5*, 3758–3761. [[CrossRef](#)]
36. Houg, H.-S.H.; Hritz, D.; Kanesa-thasan, N. Quantitative detection of dengue 2 virus using fluorogenic RT-PCR based on 3%-noncoding sequence. *J. Virol. Methods* **2000**, *86*, 1–11. [[CrossRef](#)]
37. Chao, D.-Y.; Davis, B.S.; Chang, G.-J.J. Development of multiplex real-time reverse transcriptase PCR assays for Detecting Eight Medically Important Flaviviruses in Mosquitoes. *J. Clin. Microbiol.* **2007**, *45*, 584–589. [[CrossRef](#)]
38. Darwish, N.T.; Alias, Y.B.; Khor, S.M. An introduction to dengue-disease diagnostics. *TrAC Trend. Anal. Chem.* **2015**, *67*, 45–55. [[CrossRef](#)]
39. Zaytseva, N.V.; Montagna, R.A.; Baeumner, A.J. Microfluidic biosensor for the serotype-specific detection of dengue virus RNA. *Anal. Biochem.* **2005**, *77*, 7520–7527. [[CrossRef](#)]
40. Chen, S.-H.; Chuang, Y.-C.; Lu, Y.-C.; Lin, H.-C.; Yang, Y.-L.; Lin, C.-S. A method of layer-by-layer gold nanoparticle hybridization in a quartzcrystal microbalance DNA sensing system used to detect dengue virus. *Nanotechnology* **2009**, *20*, 215501. [[CrossRef](#)]
41. Yin, Z.; Ramshani, Z.; Waggoner, J.J.; Pinsky, B.A.; Senapati, S.; Chang, H.-C. A non-optical multiplexed PCR diagnostic platform for serotype-specific detection of dengue virus. *Sens. Actuator B-Chem.* **2020**, *310*, 127854. [[CrossRef](#)]

